8. *Ex Situ Conservation: Present Status and Future Priorities* (A.I.D. Report, Bureau for Science and Technology, Washington, DC, 1990).
9. D. Wood, *Food Policy*, 167 (May 1988).
10. K. L. Tao, J. T. Williams, D. H. van Sloten, *Environ. Conserv.* **16**, 311 (1989).
11. J. I. Cohen, D. L. Plucknett, N. J. H. Smith, K. A. Jones, *Biotechnology* **6**, 387 (1988).
12. D. R. Marshall, in *Plant Population Genetics, Breeding, and Genetic Resources*, A. D. H. Brown, M. T. Clegg, A. L. Kahler, B. S. Weir, Eds. (Sinauer, Amherst, MA, 1990), pp. 367–388.
13. M. A. Smith and A. Y. Blumberg, *Diversity* **6**, 7 (1990).
14. See, for example, T. T. Chang [*Crop Exploration and Utilization of Genetic Resources*, Proceedings of International Symposium, 6 to 12 December 1986, Changhua, Taiwan (Taichung District Agricultural Improvement Station, Taiwan, Republic of China, 1987), pp. 225–231].
15. G. P. Nabhan, *Enduring Seeds* (North Point Press, San Francisco, 1989).
16. *Managing Global Genetic Resources: The U.S. National Plant Germplasm System* (National Academy of Sciences, Washington, DC, 1991).
17. M. Goodman, *J. Hered.* **81**, 11 (1990).
18. J. T. Williams, in *Biotic Diversity and Germplasm Preservation, Global Imperatives*, L. Knutson and A. K. Stoner, Eds. (Kluwer, Netherlands, 1989), pp. 81–96.
19. Annual Report (IRRI, Manila, Philippines, 1986); Program Report (IRRI, Manila, Philippines, 1989).
20. *The Biodiversity Conservation Strategy Program, Program Description* (World Resources Institute, Washington, DC, May, 1990).
21. P. H. Abelson, *Science* **253**, 117 (1991).
22. "Policy Statement on Cooperative Research and Development Agreements and Intellectual Property Licensing," in *PHS Technology Transfer Directory* (Office of Technology Transfer, NIH, Bethesda, MD, 1989), section 8, pp. 107–139.
23. K. A. Dahlberg, *Conserv. Biol.* **1**, 311 (1987).
24. J. I. Cohen, J. B. Alcorn, C. S. Potter, *Econ. Bot.* **45**, 190 (1991).
25. D. A. Vaughan and L. A. Sitch, *BioScience* **41**, 22 (1991).
26. O. H. Frankel, "Perspectives on genetic resources," in *CIMMYT 1988 Annual Report: Delivering Diversity* (CIMMYT, Mexico, 1988).
27. We thank R. Bissell, Assistant Administrator for Science and Technology, A.I.D., for direction and support; genetic resource unit directors at CGIAR centers and directors of U.S. regional plant introduction and conservation centers for providing data on accessions; J. Schweitzer, M. Horne, and L. Withers for preparation of report; and T. T. Chang, R. Gerrits, B. Rall, D. Wildt, C. Sperling, M. Goodman, S. Eberhart, B. Maunder, J. Spears, S. Krugman, M. Strauss, J. Abramovitz, and M. Symington for review and consultation.

Research Articles

Atomic Structure of Acetylcholinesterase from *Torpedo californica*: A Prototypic Acetylcholine-Binding Protein

JOEL L. SUSSMAN,* MICHAL HAREL, FELIX FROLOW, CHRISTIAN OEFNER,† ADRIAN GOLDMAN,‡ LILLY TOKER, ISRAEL SILMAN*

The three-dimensional structure of acetylcholinesterase from *Torpedo californica* electric organ has been determined by x-ray analysis to 2.8 angstrom resolution. The form crystallized is the glycolipid-anchored homodimer that was purified subsequent to solubilization with a bacterial phosphatidylinositol-specific phospholipase C. The enzyme monomer is an α/β protein that contains 537 amino acids. It consists of a 12-stranded mixed β sheet surrounded by 14 α helices and bears a striking resemblance to several hydrolase structures including dienelactone hydrolase, serine carboxypeptidase-II, three neutral lipases, and haloalkane dehalogenase. The active site is unusual because it contains Glu, not Asp, in the Ser-His-acid catalytic triad and because the relation of the triad to the rest of the protein approximates a mirror image of that seen in the serine proteases. Furthermore, the active site lies near the bottom of a deep and narrow gorge that reaches halfway into the protein. Modeling of acetylcholine binding to the enzyme suggests that the quaternary ammonium ion is bound not to a negatively charged "anionic" site, but rather to some of the 14 aromatic residues that line the gorge.

THE PRINCIPAL BIOLOGICAL ROLE OF ACETYLCHOLINESTERASE (AChE, acetylcholine hydrolase, E.C. 3.1.1.7) is termination of impulse transmission at cholinergic synapses by rapid hydrolysis of the neurotransmitter acetylcholine (ACh) (*1*).

$$CH_3COOCH_2CH_2N^+(CH_3)_3 + AChE \rightarrow CH_3CO\text{–}AChE$$
$$+ HOCH_2CH_2N^+(CH_3)_3 \rightarrow CH_3COO^- + H^+ + AChE$$

In keeping with this requirement, AChE has a remarkably high specific activity, especially for a serine hydrolase [for a review, see (*2*)], and functions at a rate approaching that of a diffusion-controlled reaction (*3*). The powerful acute toxicity of organophosphorus poisons (as well as of carbamates and sulfonyl halides, which function analogously) is primarily because they are potent inhibitors of AChE (*4*). They inhibit AChE by forming a covalent bond to a Ser residue in the active site (*2*). AChE inhibitors are used in treatment of various disorders such as myasthenia gravis and glaucoma (*5*), and their use has been proposed as a possible therapeutic approach in the management of Alzheimer's disease (*6*). Knowledge of the three-dimensional (3-D) structure of AChE is therefore

J. L. Sussmann, M. Harel, F. Frolow, C. Oefner, and A. Goldman are in the Department of Structural Chemistry and L. Toker and I. Silman are in the Department of Neurobiology at The Weizmann Institute of Science, Rehovot 76100, Israel.

*To whom correspondence should be addressed.
†Visiting scientist at the Weizmann Institute of Science. Permanent address: F. Hoffmann–La Roche Ltd., Central Research Unit, CH-4002 Basel, Switzerland.
‡Visiting scientist at the Weizmann Institute of Science. Permanent address: Waksman Institute, Rutgers University, New Brunswick, NJ 08855.

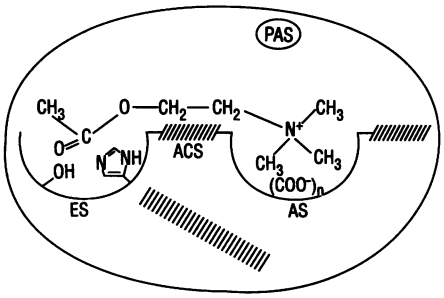

Fig. 1. Schematic representation of the binding sites of AChE based upon previous kinetic, spectroscopic, and chemical modification studies: ES, esteratic site; AS, anionic substrate binding site; ACS, active site–selective aromatic cation binding site; and PAS, peripheral anionic binding site or sites. The hatched areas represent putative hydrophobic binding regions. The ACh molecule is shown spanning the esteratic and anionic sites of the catalytic center. Imidazole and hydroxyl side chains of His and Ser are shown within the esteratic site. Within the anionic site, $(COO^-)_n$ represents six to nine putative negative charges.

essential for understanding its remarkable catalytic efficacy, for rational drug design, and for developing therapeutic approaches to organophosphate poisoning. Furthermore, information about the ACh-binding site of AChE should help in understanding the molecular basis for the recognition of ACh by other ACh-binding proteins such as the various ACh receptors (*7*).

The various oligomeric forms of AChE in the electric organ of the electric fish, *Electrophorus* and *Torpedo*, are structurally homologous to those in vertebrate nerve and muscle (*8*). Highly purified preparations from these abundant sources of AChE (*9*) have taught us much about the number and arrangement of subunits and modes of anchoring to the surface membrane of these molecular forms (*10*).They have also yielded considerable information concerning the surface topography of AChE (*11*) and its mechanism of action (*2*).

Early kinetic studies indicated that the active site of AChE contains two subsites, the "esteratic" and "anionic" subsites (*12*), corresponding, respectively, to the catalytic machinery and the choline-binding pocket. The esteratic subsite is believed to resemble the catalytic subsites of other serine hydrolases (*13, 14*). The active site serine, with which organophosphates react, has been unequivocally established to be Ser^{200} in *T. californica* AChE (*15*). Both kinetic and chemical studies (*16*) implicate a His residue in the active site. The anionic subsite binds the charged quaternary group of the choline moiety of ACh, and is believed to bind both quaternary ligands, such as edrophonium (*17*) and *N*-methylacridinium (*18*), which act as competitive inhibitors, and quaternary oximes, which often serve as effective reactivators of organophosphate-inhibited AChE (*13*). Cohen and co-workers (*19*) have suggested, on the basis of studies in which cationic and uncharged homologs of ACh were used, that the "anionic" subsite is, in fact, uncharged and lipophilic. Chemical modification and spectroscopic studies also support the presence of aromatic residues in the active site of AChE (*20–23*).

In addition to the two subsites of the catalytic center, AChE possesses one or more additional binding sites for ACh and other quaternary ligands (Fig. 1). Such "peripheral" anionic sites, clearly distinct from the choline-binding pocket of the active site, have been proposed (*18, 24*) and were firmly established by Taylor and Lappi (*25*) by use of the fluorescent probe propidium. It acts as an uncompetitive inhibitor and binds at a site clearly distinct from that occupied by the monoquaternary competitive inhibitors mentioned above. Reiner and co-workers (*26*) suggested that this is the site involved in the substrate inhibition characteristic of AChE. For a recent review of this complex literature, see (*2*).

The first AChE crystals obtained were of a tetrameric form purified from electric organ tissue of *Electrophorus electricus* (*27*). Although preliminary characterization of these crystals was reported by Chothia and Leuzinger (*28*) and, more recently, by Schrag *et al.* (*29*), no structural data have yet been presented.

Structure determination. In *Torpedo*, a major form of AChE is a homodimer bound to the plasma membrane through covalently attached phosphatidylinositol (PI) (*10*). This dimer has a simpler quaternary structure than *Electrophorus* AChE, and its sequence and the arrangement of its intrachain disulfides have been determined (*15, 30, 31*). The PI is attached to the COOH-terminus of each monomer through an intervening oligosaccharide, with the diglyceride moiety of the PI serving as the hydrophobic anchor (*10*). Thus the dimer can be selectively solubilized by a bacterial PI-specific phospholipase C (*32*). This mild procedure also achieves significant purification before affinity chromatography. We were thus able to

Table 1. Crystallographic data. The crystals formed in space group $P3_121$, one monomer per asymmetric unit [unit cell constants $a = b = 110$ Å and $c = 135$ Å at room temperature (RT, ~20°C) and $a = b = 113$ Å and $c = 137$ Å at 0°C]. The resolution limit was 2.8 Å for all of the crystals studied. X-ray intensities were collected at room temperature for a native crystal and for the two derivatives, with a Siemens/Xentronics area detector installed on a Rigaku rotating-anode generator operating at 40 kV and 250 mA with a graphite monochromator. In addition, a native data set, collected at 0°C, was used for refinement. Each data set was collected from a single crystal. Data frames of 0.25° with an exposure time of 70 s were collected and processed with the XENGEN (*75*) and XDS (*76*) software packages. All subsequent crystallographic calculations were performed with the CCP4 computing package (from the Daresbury laboratory, United Kingdom) including the Dickerson-type refinement (*77*) for heavy-atom parameters as implemented in the program PHASE. The anomalous differences of both the uranyl and the mercury (mercuric acetate) derivative were included in the phasing. For the MIR phasing, the mean figure of merit was 0.59 for all reflections and 0.32 for the highest resolution shell. After solvent flattening the mean figure of merit was 0.80 for all reflections and 0.68 for the highest resolution shell. The mean phase change between MIR and solvent flattening was 32° for all reflections and 53° for the highest resolution shell.

Parameter	Derivative			
	Native (0°C)	Native (RT)	$UO_2(NO_3)_2$ (RT)	$HgAc_2$ (RT)
Measurements (No.)	83,667	41,463	44,736	43,413
Unique reflections				
Number	23,587	22,523	23,631	24,297
Completeness (percent)	90	89	93	96
R_{sym} (percent)*	10.4	10.3	11.5	11.1
R_{iso} (percent)†			17.7	15.1
MIR phasing, 15 to 2.8 Å				
R_{cullis} (percent)‡			43.9	65.4
RMS f_H/E_{iso}§			3.16/3.00	1.35/1.56
RMS f''_{calc}/E_{ano}§			0.71/0.40	0.25/0.26
Sites (no.)			6	4

*$R_{sym} = \Sigma(|I - \langle I\rangle|)/\Sigma\langle I\rangle$. †$R_{iso} = \Sigma(||F_{PH}| - |F_P||)/\Sigma|F_P|$. ‡$R_{cullis} = (\Sigma||F_{PH} \pm F_P| - F_{H(calc)}|)/(\Sigma|F_{PH} - F_P|)$ for centric reflections. §All reflections/highest resolution range; RMS, root-mean-square.

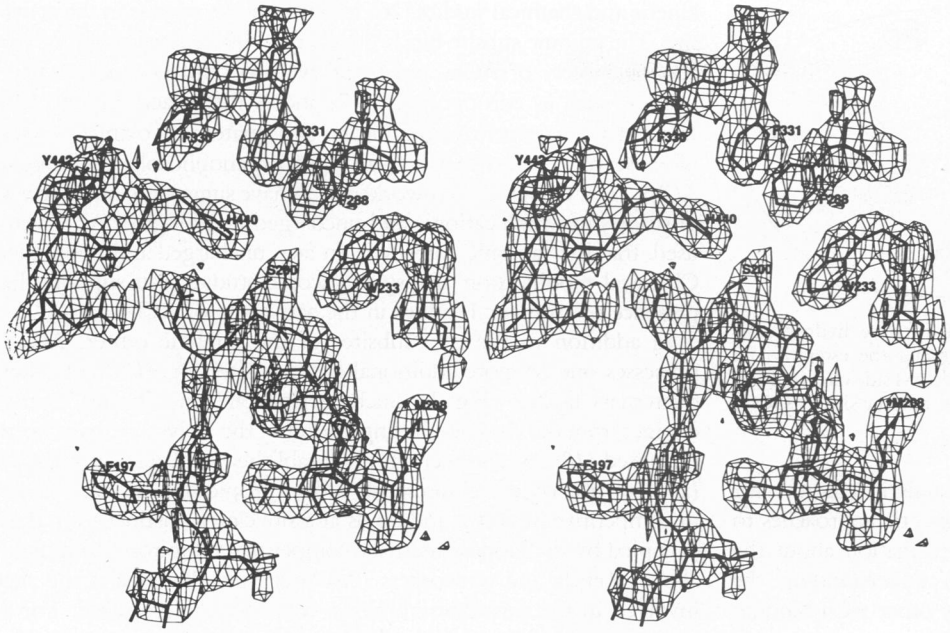

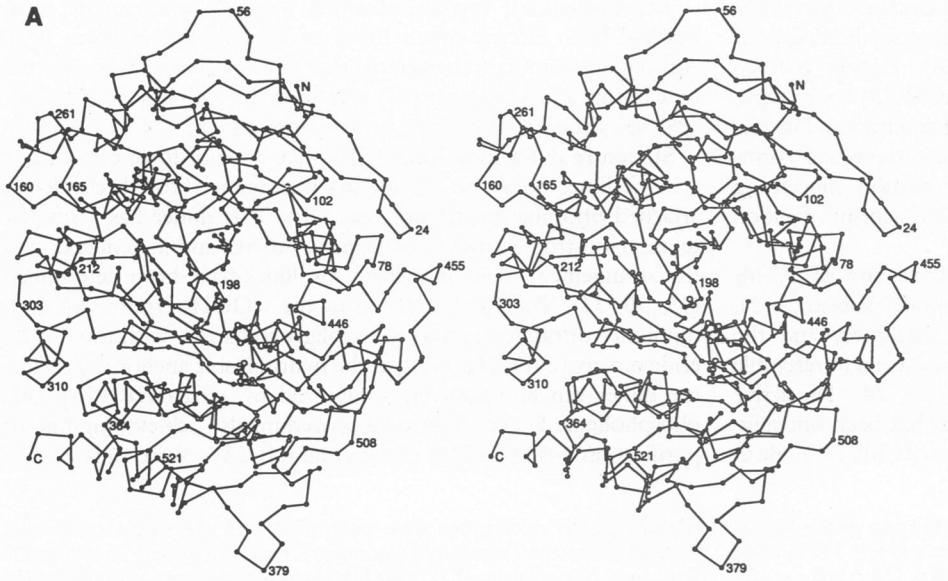

obtain large amounts of pure, unnicked enzyme for crystallization. We earlier reported preliminary crystallographic characterization of crystals of this form of AChE obtained from polyethyleneglycol (PEG) 200 (*33*).

Recently we obtained a crystal form more suitable for x-ray analysis (*34*). AChE, purified as already described (*33*), was crystallized at 19°C, with the use of standard vapor diffusion techniques in hanging drops (*35*) with 61 percent saturated ammonium sulfate, 360 mM Na,K-phosphate buffer, pH 7.0, as the precipitating agent and a protein concentration of ~11 mg/ml. Single crystals grew within a few weeks to dimensions of 0.8 mm by 0.4 mm by 0.4 mm. They belong to space group $P3_121$, contain one mono-

Fig. 2 (top). Representative portion, displayed in stereo, of the MIR-WANG 2.8 Å electron density map of AChE, in the vicinity of the active site (*78*). The current refined atomic model is superimposed. The Oγ of Ser^{200} is seen to lie at the elbow of the strand-turn-helix motif within hydrogen-bonding distance of His^{440}. Glu^{327}, the third member of the catalytic triad cannot be seen as it is out of the plane of the figure. Note the large number of aromatic residues in the immediate vicinity of the active site serine. **Fig. 3 (bottom).** (**A**) Stereo Cα trace of the AChE monomer looking into the active site gorge. Residues in the catalytic triad are indicated by solid black lines. The orientation of the trace is similar to that of the CPDW-II trace in (*46*). (**B**) Stereo ribbon diagram made with the RIBBON program (*79*), oriented as in (A). The amino terminus is located at the top right, and the carboxyl terminus at the lower left. The 12-stranded β sheet is approximately parallel to the plane of the figure, with its convex surface pointing up. The sheet is sandwiched between six helices, two on its concave surface (underneath in this view) and four on its convex surface. The other eight helices all occur in loops above the sandwich. (**C**) Secondary-structure cartoon showing the topology of AChE, with the β sheets represented by gray arrows and the α helices by rods. The dashed vertical lines indicate that the central eight-stranded mixed β sheet makes relatively few hydrogen bonds to either the first or the last β-hairpin loops. The numbering of the central β sheet corresponds to that of the eight-stranded β structure of DLH (*45*). Several helical stretches are found between strands 6 to 7 and 7 to 8 (see Fig. 4); for the sake of clarity, only the last helix is displayed in each case. The filled circles indicate the positions of the catalytic triad; Ser^{200} occurs after strand 5, Glu^{327} after strand 7, and His^{440} after strand 8.

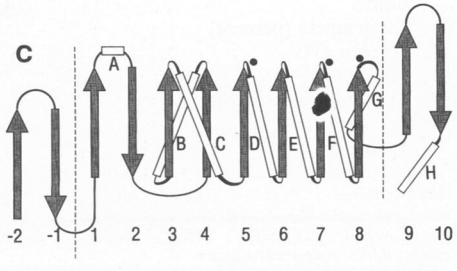

mer per asymmetric unit, and diffract to 2.6 Å resolution. Compared with the crystal form grown from PEG 200 (*33*), the trigonal crystals grow more reproducibly, are mechanically more robust, and survive longer in the x-ray beam (Table 1).

The structure was solved by the multiple isomorphous replacement (MIR) method (Table 1) followed by three cycles of solvent flattening (*36*) and phase combination to improve the map (Fig. 2). An initial AChE model comprising 505 out of a total of 537 residues in the polypeptide chain (*37*) was obtained by applying the fragment retrieval option, DGNL, to fit fragments from the Brookhaven Protein Data Bank (*38*) to the skeletonized electron density distribution generated by BONES as implemented in the program FRODO (*39*). One of the two mercury sites of the $HgAc_2$ (mercuric acetate) derivative (see Table 1) is buried in the protein's interior. Biochemical studies had previously shown that several thiol reagents, including the organomercurial, *p*-chloromercurisulfonic acid, inhibit *Torpedo* AChE (*40*). The sulfhydryl of Cys^{231} is the only free thiol in the enzyme (*31*) and seemed, therefore, a reasonable attachment site for a mercury derivative. Since kinetic constants suggested that the sulfhydryl modified is relatively inaccessible, we looked near the buried mercury atom for densities whose shape corresponded to the sequence Cys^{231}-Pro^{232}-Trp^{233}. When this sequence proved to fit the observed density satisfactorily, we built out from the tripeptide in both directions. The amino acid sequence could be fitted accurately to the electron density at all points, and bifurcations were observed, as might be predicted, at the sites of the three intrachain disulfides (*31*). The initial *R* factor for 15 to 2.8 Å resolution data based on these 505 residues was 0.43 before any crystallographic refinement.

A preliminary refinement with the simulated annealing program X-PLOR (*41*) yielded calculated phases that were used to produce a new map, which revealed an additional 21 of the missing amino acid residues. Refinement was continued with X-PLOR in conjunction with PROFFT (*42*), decreasing the *R* factor to 0.186 for all data ($F > 0\sigma$) from 6.0 to 2.8 Å resolution. The present model, consisting of 526 residues and 71 water molecules, maintains good stereochemistry; it has an root-mean-square deviation in bond lengths of 0.021 Å and in bond angles of 4.0°. Eighty-one atoms, belonging to side chains of 27 polar surface residues that were not seen in the electron density map even after being omitted, were excluded from the refinement. The coordinates have been deposited in the Brookhaven Protein Data Bank (*38*).

General structure. The molecule has an ellipsoidal shape with dimensions ~45 Å by 60 Å by 65 Å. It belongs to the class of α/β proteins (*43*) and consists of a 12-stranded central mixed β sheet surrounded by 14 α helices (Figs. 3 and 4). The first and last pairs of strands each form β-hairpin loops that are only loosely hydrogen-bonded to the eight central, superhelically twisted strands (Fig. 3B). Viewed along its axis, the sheet curves ~180°, while viewed perpendicular to its axis, the first and last strands cross each other at ~90°. Of the 14 helices, two of the longer ones, namely αF and αH, are bent close to their interhelix disulfide bridge. The α-helical content of 30 percent and β-sheet content of 15 percent observed in the crystal structure are in reasonable agreement with those estimated from circular dichroism measurements (*44*).

The AChE homodimer, whose subunits are related by a crystallographic twofold axis, appears to be held together by a four-helix bundle composed of helices αF'3 and αH from each subunit (Fig. 5). The only interchain disulfide involves the carboxyl-terminal Cys^{537} (*31*). The three carboxyl-terminal residues and the oligoglycan extension of the membrane-anchoring domain (*37*) are not visible in the electron density map, most probably because they are disordered. Residues 1 to 3 and an exposed loop from 485 to 489 are also not seen, presumably for the same reason. At Asn^{416}, one of four putative glycosylation sites (*30*), there is electron density that may correspond to the proximal sugar moiety.

The overall structure of AChE is strikingly similar to those of dienelactone hydrolase (DLH) (*45*) and wheat serine carboxypeptidase-II (CPDW-II) (*46*). β strands 1 to 8 of AChE (using the numbering of Fig. 3C) have the same topology as the eight-stranded β sheet of DLH, while CPDW-II has the same topology with an additional β loop inserted before the last strand. As pointed out by Liao and Remington (*46*), CPDW-II has a similar fold to two neutral lipases, human pancreatic (HPL) (*47*) and *Mucor miehei* (*48*), as well as to carboxypeptidase-B (*49*). In AChE, five of the six crossover connections between the parallel strands, strands 4 to 8 in AChE, are of the common right-handed β/α/β or β/loop/β type (*50*), as is the case in the corresponding crossovers in HPL (*47*). The last crossover, which consists of 67 residues and contains two α-helical segments is, as in HPL, of the very rare left-handed type. AChE also possesses remarkable sequence homology in its active-site region to a lipase from *Geotrichum candidum* (*51*), whose 3-D structure has just been determined (*52*). The structure of an additional enzyme, haloalkane dehalogenase, which displays structural similarity to AChE, has also just been reported (*53*). The similarity of these enzymes has been studied in more detail (*54*).

Active site. The existence of a catalytic triad in AChE has been the subject of controversy (*2*). The earlier identification of Ser^{200} as the active-site serine of *T. californica* AChE (*15*) has recently been supplemented by the designation of His^{440} as the catalytic His

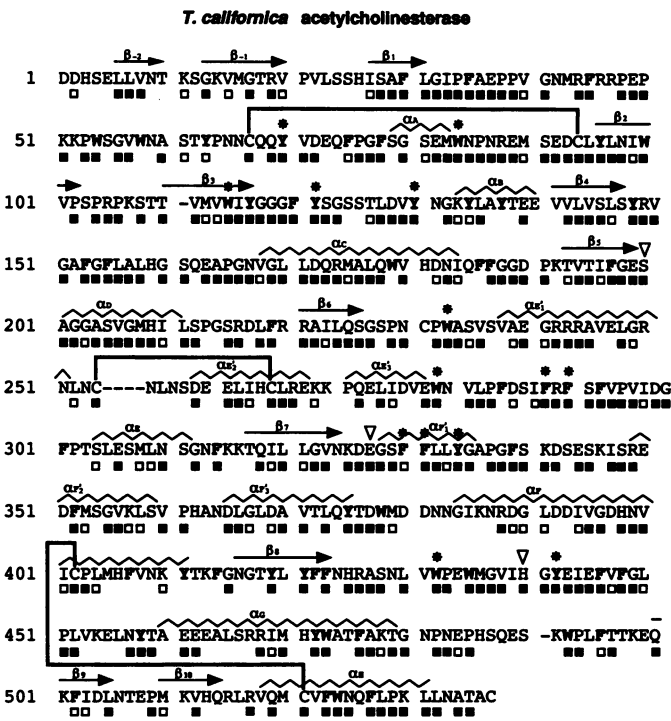

Fig. 4. Amino acid sequence (*78*) and secondary structure of the polypeptide chain of PI-anchored AChE from *T. californica* [taken from (*15, 30, 37*)]. Aromatic residues are in bold, with those whose side chain faces the active site pocket being starred (*). The members of the catalytic triad are marked with an open arrowhead. Sequence homology was examined between this AChE and four others [*T. marmorata*, mouse, human, and bovine (*55*)]. Dashes indicate gaps in the *Torpedo* sequence relative to the mammalian sequences. All identical residues, that is conserved in all five sequences, are marked by (■). Similar residues are marked by (□), where similarity is considered to be present if G is replaced by A (or vice versa), T by S, D by E, K by R, and L by V, I or M. The pairs of cysteines in the conserved disulfide bridges (*31*) are connected appropriately. β Strands and α-helical regions are indicated by arrows and by zigzag lines, respectively, above the amino acid sequence.

residue on the basis of sequence comparison (*55*) and site-directed mutagenesis (*56*). Our chain tracing clearly supports this assignment by placing His^{440} close to Ser^{200}; Glu^{327} is also near His^{440}. The three residues form a planar array that resembles the catalytic triad of chymotrypsin (Cht) and other serine proteases (*57*) (Fig. 6A). There are, however, two important differences:

1) AChE and the above-mentioned lipase from *Geotrichum candidum* (*52*), are, to the best of our knowledge, the first published cases of Glu occurring instead of Asp in a catalytic triad.

2) As in CPDW-II, DLH, and the neutral lipases, which have a similar fold to AChE (see above), this triad is of the opposite "handedness" to that of Cht. The change in hand is equivalent to keeping the position of the Ser Oγ, histidine imidazole ring, and acid carboxylate group approximately constant, while rotating the rest of the molecule about the line joining Ser Cβ to His Cγ. This change reverses the direction of the polypeptide backbone around the His and Ser residues (Fig. 6A). This structure suggests that the oxyanion hole, which is formed by the amide NH of the active site Ser in the serine proteases (amino terminal), would be formed by the amide NH of the following residue in AChE, Ala^{201} (carboxyl terminal), as appears to be the case for HPL (*47*) and for the other structurally related hydrolases (*54*). All three triad residues occur within highly conserved regions of the sequence (Fig. 4) and, as is typical of active sites in α/β proteins (*58*), are in loops following the carboxyl termini of β strands.

The active site gorge. The most remarkable feature of the structure is a deep and narrow gorge, ~20 Å long, that penetrates halfway into the enzyme and widens out close to its base (Fig. 7A). We have named this cavity the "active site gorge" because it contains the AChE catalytic triad. The Oγ atom of Ser^{200}, which can be seen from the surface of the enzyme (Fig. 7B), is ~4 Å above the base of the gorge. Fourteen aromatic residues line a substantial portion of the surface of the gorge (~40 percent) (Figs. 2, 4, 7, and 8). These residues and their flanking sequences, which are highly conserved in AChE's from different species (Fig. 4), come primarily from loops between β1 and β2, β3 and β4, β6 and β7, β7 and β8, and those after β8 (Fig. 3C). Residues as far apart as Asn^{66} and Ile^{444} contribute to the lining and base of the gorge and are synthesized on the first exon, which codes for residues 1 to 480 (*59*). The gorge contains only a few acidic residues, which include Asp^{285} and Glu^{273} at the very top, Asp^{72}, hydrogen bonded to Tyr^{334}, about halfway down, and Glu^{199} near the bottom.

The presence of tryptophan in the active site of AChE was predicted by spectroscopic and chemical modification studies (*21, 23*). The recent affinity labeling study of Weise *et al.* (*60*) in fact identified Trp^{84} as part of the putative anionic (choline) binding site. An earlier photoaffinity labeling study implicated a peptide in electric eel AChE, homologous to *Torpedo* Gly^{328}-Ser^{329}-Phe^{330}-Phe^{331}, as part of the binding site (*61*). The observation of Tyr residues adjacent to the catalytic site agrees with chemical modification studies (*20–22*). The hydroxyl groups of Tyr^{121} (halfway up) and Tyr^{130} (at the bottom) point into the gorge.

Despite the structural complexity of the gorge and the flexibility of the natural substrate, ACh (*62*), a good fit of the extended, all-trans conformation of ACh was obtained by manual docking (*63*). Specifically, the acyl group was positioned to make a tetrahedral bond with the Oγ of Ser^{200} while the quaternary group of the choline moiety was placed within van der Waals distance (~3.5 Å) of Trp^{84} (Fig. 6B). The model suggests that the oxyanion hole (*57*) would be formed by the main chain nitrogens of Gly^{118}, Gly^{119}, and Ala^{201} interacting with the carbonyl oxygen, and that the ester oxygen may interact with the imidazole of His^{440}. The fact that the amide nitrogen of Ala^{201}, and not that of Ser^{200}, contributes to the oxyanion hole is consistent with the reversed topology, noted above, of the catalytic triad relative to the serine proteases. Gly^{118} and Gly^{119} are part of a ten-residue conserved sequence which contains three glycines in a row; this may make the chain flexible enough to allow amide nitrogens from both Gly^{118} and Gly^{119} to be part of the oxyanion hole. Glu^{199}, which might serve as an anionic component of the substrate-binding site, appears in our model to make close

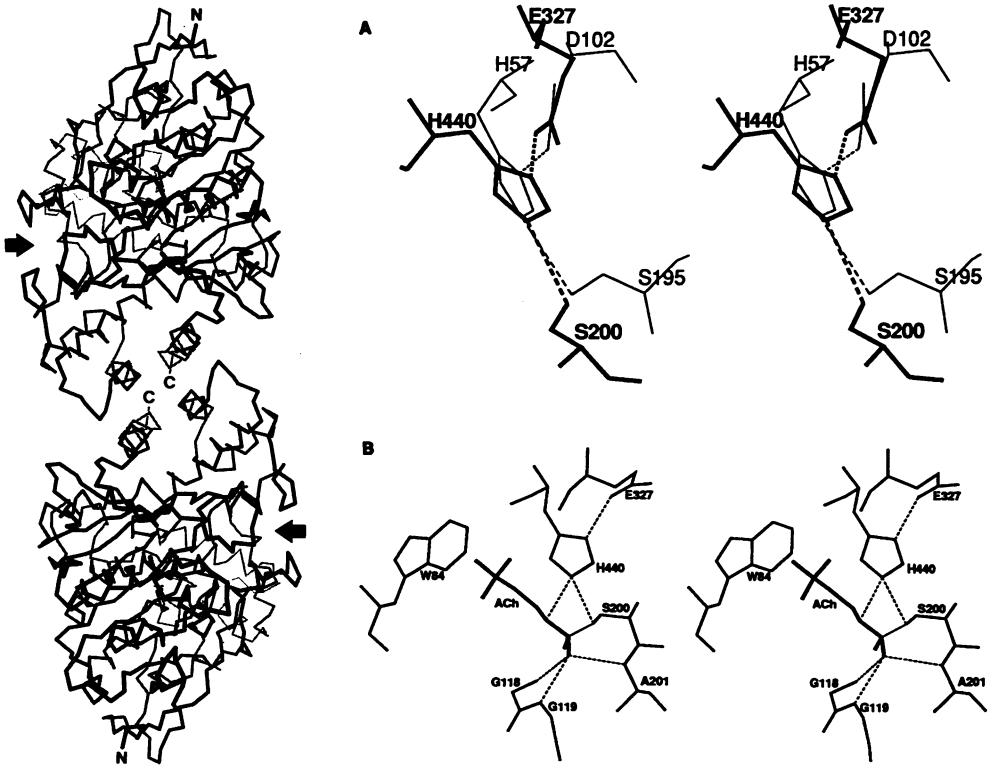

Fig. 5 (left). Cα trace of an AChE dimer, viewed down the crystallographic twofold axis. The active sites, whose positions are indicated by arrows, are ~60 Å apart. A four-helix bundle composed of α helices F′3 and H from each subunit and a short loop between α helices F3 and F are the only observed noncovalent contacts between the two subunits. The carboxyl-terminus is labeled C, and the amino terminus is labeled N. **Fig. 6 (right).** (**A**) Superposition of the catalytic triads of AChE (Ser^{200}-His^{440}-Glu^{327}) (darker) and Cht (*80*) (Ser^{195}-His^{57}-Asp^{102}) (lighter) showing that, when the imidazole rings of the histidines are superimposed, the main chains point in opposite directions at the histidine and the serine. The hydrogen bonds of the active site triads are marked by dashed lines. The distance Ser^{200} Oγ–His^{440} Nε2 is 3.1 Å; His^{440} Nδ1–Glu^{327} Oε1 is 2.5 Å. (**B**) A theoretical model for the docking of ACh onto AChE. The triad and the nearby environment, including the oxyanion hole and Trp^{84}, are shown. The thin solid line marks the bond produced in the transition state between Ser^{200} Oγ of AChE and the carbonyl carbon of ACh. Dashed lines indicate the putative hydrogen bonds.

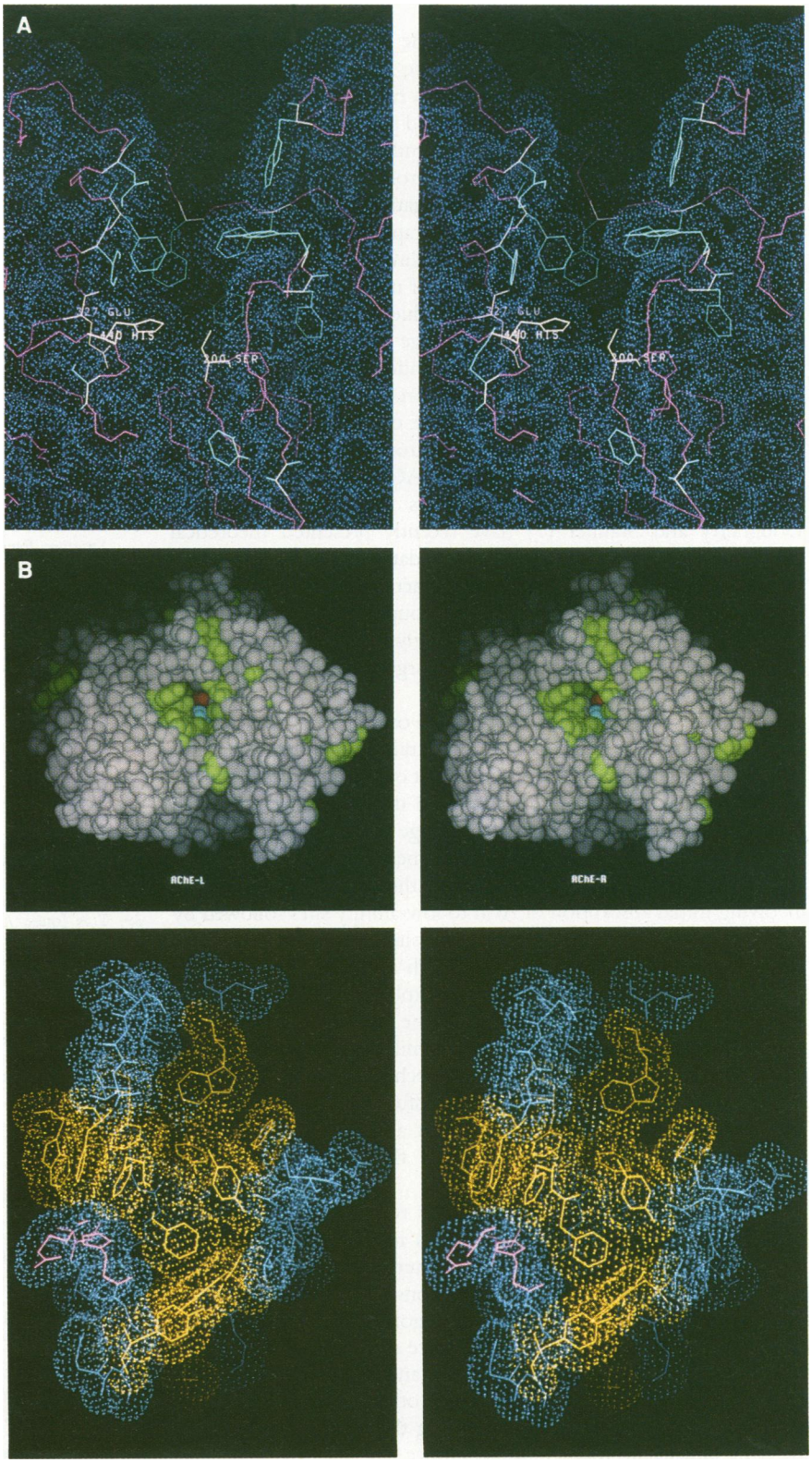

Fig. 7 (top). (**A**) Stereo drawing of a thin slice through the AChE monomer. The blue-dot van der Waals surface shows the narrow gorge leading down to the active site. The backbone is pink, the aromatic groups are light green, and the catalytic triad is white. (**B**) Space-filling stereo view of the AChE molecule looking down into the active site gorge with the MacIMDAD program. Aromatic residues are green, and the other residues are gray. Ser^{200} (red) and Glu^{199} (cyan) are visible toward the bottom of the gorge. **Fig. 8 (bottom).** Stereo representation that includes all of the residues contributing to the active site gorge. The view is rotated ~90° around the vertical axis with respect to the view shown in Fig. 7A. Aromatic residues are colored gold and the other residues are blue, both types being embellished with van der Waals dot surfaces. The catalytic triad residues are pink. This view of the gorge clearly shows that the rim on one side is much higher than on the other.

contacts (~3 Å) both to one of the quaternary methyl groups and to the α-carbon of the choline moiety. We have omitted it from Fig. 6B since it has been reported that mutating it to glutamine had little effect on the kinetic parameters (*56*). Glu^{199} appears, however, to be hydrogen-bonded, either directly or through a water molecule, to Glu^{443}. As both carboxylic acid side chains are in a hydrophobic environment in the interior of AChE, it seems likely that one or both of them are protonated. This might explain the surprising result of the mutagenesis experiment.

The high aromatic content of the walls and floor of the active site gorge, together with its dimensions, may help explain why biochemical studies have revealed a variety of hydrophobic and anionic binding sites distinct from, or overlapping, the active site. For instance, chemical modification by various reagents (*20, 64*) greatly reduces enzymic activity towards ACh either without affecting, or sometimes actually enhancing, activity towards various neutral esters. This supports the existence of hydrophobic areas distinct from the binding site for ACh. Other evidence for hydrophobic sites extending beyond or distinct from the anionic site comes from studies on the affinities and reaction rates of homologous series of organophosphate inhibitors (*65*), on the affinities of various acridine derivatives (*66*), and from studies employing resolved enantiomeric methylphosphonothioates (*67*). The complexity of the array of aromatic residues also provides candidates for a binding site for aromatic cations, the existence of which, closer to the esteratic site than the anionic site, was recently proposed (*11*). All of these results are consistent with the characteristics of the deep gorge extending up from the active site of AChE.

Two reports have used photolabeling (*68*) and affinity labeling (*60*) to identify peptide sequences, residues 251 to 264 and 270 to 278, respectively, as part of the peripheral binding site or sites for ACh and other quaternary ligands. These two neighboring peptides on the surface of the protein are close to the rim of the gorge. The complex and varied inhibitory effects of different peripheral site ligands (*2, 14, 24*) may be better understood taking into account the complex geometry of the gorge. Certain ligands may be too bulky to penetrate it, but still could partially block its entrance. The longer bisquaternary compounds, which serve as potent inhibitors, might attach at one end to the peripheral site or sites and at the other end to any one of the various aromatic residues lining the walls of the gorge. However, because of its depth, shorter bisquaternary inhibitors and oxime reactivators might bind wholly within the gorge itself.

Aromatic guidance. There has been much discussion concerning the chemical characteristics of the anionic binding site of AChE (*2*) as well as of ACh-binding proteins in general (*7*). The positive charge of ACh and of numerous potent ligands led to the designa-

tion of the site as anionic, and this was supported by the study of Nolte *et al.* (*69*), which indicated that the binding site for ACh in *Electrophorus* AChE contains six to nine negative charges. They suggested that the exceptionally high on-rate observed for quaternary ligands might thus be due to the field produced by the array of negative charges. This is somewhat similar to the "electrostatic guidance" mechanism postulated for superoxide dismutase, in which an array of positive charges guides the negatively charged superoxide radical into the active site cavity of this rapid enzyme (*70*).

The above hypothesis, though appealing, is at odds with our structure. We see only a small number of negative charges close to the catalytic site, but many aromatic residues both near the catalytic triad and on the walls of the narrow gorge leading down to it. The prototypic crystallographic study of a binding site for a quaternary ligand, that of the McPC603 myeloma protein, which binds phosphorylcholine selectively, showed that the quaternary moiety of the bound ligand was associated with three aromatic rings (*71*). Chemical modification studies of the nicotinic ACh receptor also point to involvement of aromatic residues in its ACh-binding site (*72*). Dougherty and Stauffer (*7*) have recently presented theoretical considerations, as well as experimental data obtained with model host sites, to support a preferential interaction of quaternary nitrogens with the π electrons of aromatic groups. Indeed, they suggest that aromatic groups interact more strongly with quaternary ammonium ligands than with isosteric uncharged ligands, presumably because of the polarizability of the ion.

It is, however, pertinent to ask how the overall aromatic character of the gorge might contribute to the high rate of ligand binding and, thereby, to the high catalytic activity. First of all, the hydrophobicity of the gorge would produce a low local dieletric constant, which could result in a higher effective local charge than might be predicted from the small number of acidic groups nearby (*69*). More important, the aromatic lining may permit the use of a mechanism involving initial absorption of ACh to low-affinity sites followed by two-dimensional diffusion to the active site (*73*). Rosenberry and Neumann (*74*) earlier proposed that such a mechanism, involving multiple negatively charged sites, might explain the high on-rates for ligand-binding displayed by AChE. The aromatic lining could function analogously by providing a similar array of low-affinity binding sites (an "aromatic guidance" mechanism). The ACh, once trapped at the top of the well, could diffuse rapidly down to the active site. This same mechanism might also provide an efficient means of achieving rapid clearance of the quaternary reaction product, choline.

The crystal structure of AChE clearly reveals that the choline-binding anionic subsite is misnamed, as it contains at most one formal negative charge. Instead the quaternary moiety of choline appears to bind chiefly through interactions with the π electrons in the aromatic residues on AChE. The gorge is so deep and its aromatic surface is so extensive that there must be many different ways and places for substrate, agonists, and inhibitors to bind to AChE. It will be intriguing to see if other proteins that bind quaternary ammonium ligands, including the ACh receptors, have the same unusual aromatic binding surface.

REFERENCES AND NOTES

1. E. A. Barnard, in *The Peripheral Nervous System*, J. I. Hubbard, Ed. (Plenum, New York, 1974), pp. 201–224; B. Katz, *Nerve, Muscle, and Synapse* (McGraw-Hill, New York, 1966).
2. D. M. Quinn, *Chem. Rev.* **87**, 955 (1987).
3. B. B. Hasinoff, *Biochim. Biophys. Acta* **704**, 52 (1982); M. Bazelyansky, C. Robey, J. F. Kirsch, *Biochemistry* **25**, 125 (1986).
4. G. B. Koelle, *Cholinesterases and Anticholinesterase Agents*, vol. 12 of *Handbuch der Experimentellen Pharmakologie* (Springer-Verlag, Berlin, 1963).
5. P. Taylor, in *The Pharmacological Basis of Therapeutics*, A. G. Gilman, T. W. Rall, A. Nies, P. Taylor, Eds. (Pergamon, New York, 1990), pp. 131–149.
6. M. Hallak and E. Giacobini, *Neuropharmacology* **28**, 199 (1989).
7. D. A. Dougherty and D. A. Stauffer, *Science* **250**, 1558 (1990).
8. S. Bon, M. Vigny, J. Massoulie, *Proc. Natl. Acad. Sci. U.S.A.* **76**, 2546 (1979).
9. D. Nachmansohn and E. Neumann, *Chemical and Molecular Basis of Nerve Activity* (Academic Press, New York, 1975).
10. I. Silman and A. H. Futerman, *Eur. J. Biochem.* **170**, 11 (1987).
11. H. A. Berman and K. Leonard, *Biochemistry* **29**, 10640 (1990).
12. D. Nachmansohn and I. B. Wilson, *Adv. Enzymol.* **12**, 259 (1951).
13. H. C. Froede and I. B. Wilson, *The Enzymes* **5**, 87 (1971).
14. T. L. Rosenberry, *Adv. Enzymol.* **43**, 103 (1975).
15. K. MacPhee-Quigley, P. Taylor, S. Taylor, *J. Biol. Chem.* **260**, 12185 (1985).
16. I. B. Wilson and F. Bergmann, *ibid.* **186**, 683 (1950); R. Roskoski, *Biochemistry* **13**, 5141 (1974).
17. I. B. Wilson and C. Quan, *Arch. Biochem. Biophys.* **73**, 131 (1958).
18. G. Mooser and D. S. Sigman, *Biochemistry* **13**, 2299 (1974).
19. S. G. Cohen *et al.*, *Biochim. Biophys. Acta* **997**, 167 (1989).
20. S. Fuchs, D. Gurari, I. Silman, *Arch. Biochem. Biophys.* **165**, 90 (1974).
21. S. Blumberg and I. Silman, *Biochemistry* **17**, 1125 (1978).
22. J. D. Page and I. B. Wilson, *J. Biol. Chem.* **260**, 1475 (1985).
23. M. P. Goeldner and C. G. Hirth, *Proc. Natl. Acad. Sci. U.S.A.* **77**, 6439 (1980); M. Shinitzky, Y. Dudai, I. Silman, *FEBS Lett.* **30**, 125 (1973).
24. F. Bergmann, I. B. Wilson, D. Nachmansohn, *Biochim. Biophys. Acta* **6**, 217 (1950); J. P. Changeux, *Mol. Pharmacol.* **2**, 369 (1966); B. Belleau, V. DiTullio, Y. H. Tsai, *ibid.* **6**, 41 (1970).
25. P. Taylor and S. Lappi, *Biochemistry* **14**, 1989 (1975).
26. E. Reiner, N. Aldridge, V. Simeon, Z. Radic, P. Taylor, in *Cholinesterases: Structure, Function, Mechanism, Genetics and Cell Biology*, J. Massoulie *et al.*, Eds. (American Chemical Society, Washington, DC, 1991), pp. 227–234.
27. W. Leuzinger and A. L. Baker, *Proc. Natl. Acad. Sci. U.S.A.* **57**, 446 (1967).
28. C. Chothia and W. Leuzinger, *J. Mol. Biol.* **97**, 55 (1975).
29. J. Schrag *et al.*, *J. Biol. Chem.* **263**, 9795 (1988).
30. M. Schumacher *et al.*, *Nature* **319**, 407 (1986).
31. K. MacPhee-Quigley, T. S. Vedvick, P. Taylor, S. S. Taylor, *J. Biol. Chem.* **261**, 13565 (1986).
32. A. H. Futerman, M. G. Low, I. Silman, *Neurosci. Lett.* **40**, 85 (1983).
33. J. L. Sussman *et al.*, *J. Mol. Biol.* **203**, 821 (1988).
34. J. L. Sussman, M. Harel, F. Frolow, I. Silman, *Proceedings of the Seventh Annual Chemical Defense and Bioscience Review*, Columbia, MD, 1989, pp. 309–316; J. L. Sussman *et al.*, in *Cholinesterases: Structure, Function, Mechanism, Genetics and Cell Biology*, J. Massoulie *et al.* (American Chemical Society, Washington, DC, 1991), pp. 7–11.
35. A. McPherson, *Methods Biochem. Anal.* **23**, 249 (1976).
36. B. C. Wang, *Methods Enzymol.* **115**, 90 (1985).
37. G. Gibney *et al.*, *J. Biol. Chem.* **263**, 1140 (1988).
38. F. C. Bernstein *et al.*, *J. Mol. Biol.* **112**, 535 (1977).
39. T. A. Jones, *J. Appl. Crystallogr.* **11**, 268 (1978); J. W. Pflugrath, M. A. Saper, F. A. Quiocho, in *Methods and Applications in Crystallographic Computing*, S. Hall and T. Ashiaka, Eds. (Clarendon, Oxford, 1984), pp. 404–407; T. A. Jones and S. Thirup, *EMBO J.* **5**, 819 (1986).
40. N. Steinberg, E. Roth, I. Silman, *Biochem. Int.* **21**, 1043 (1990).
41. A. T. Brünger, J. Kuriyan, M. Karplus, *Science* **235**, 458 (1987).
42. W. A. Hendrickson and J. H. Konnert, in *Biomolecular Structure, Function, Conformation and Evolution*, R. Srinivasan *et al.*, Eds. (Pergamon, Oxford, 1981), pp. 43–57; B. C. Finzel, *J. Appl. Crystallogr.* **20**, 53 (1987); S. Sheriff, *ibid.*, p. 55.
43. M. Levitt and C. Chothia, *Nature* **261**, 552 (1976); J. S. Richardson, *Methods Enzymol.* **115**, 341 (1985).
44. P. Manavalan, P. Taylor, W. C. Johnson, Jr., *Biochim. Biophys. Acta* **829**, 365 (1985).
45. D. Pathak, K. L. Ngai, D. Ollis, *J. Mol. Biol.* **204**, 435 (1988); D. Pathak and D. Ollis, *ibid.* **214**, 497 (1990).
46. D. Liao and S. J. Remington, *J. Biol. Chem.* **265**, 6528 (1990).
47. F. K. Winkler, A. D'Arcy, W. Hunziker, *Nature* **343**, 771 (1990); K. Gubernator, K. Müller, F. K. Winkler, in *Lipases-Structure, Mechanism and Genetic Engineering*, L. Alberghina *et al.*, Eds. (VCH, Weinheim, 1991), vol. 16, pp. 9–16.
48. L. Brady *et al.*, *Nature* **343**, 767 (1990).
49. D. C. Rees, M. Lewis, W. M. Lipscomb, *J. Mol. Biol.* **168**, 367 (1983).
50. J. S. Richardson, *Proc. Natl. Acad. Sci. U.S.A.* **73**, 2619 (1976); M. J. E. Sternberg and J. M. Thornton, *J. Mol. Biol.* **105**, 367 (1976).
51. A. R. Slabas, J. Windust, C. M. Sidebottom, *Biochem. J.* **269**, 279 (1990).
52. J. D. Schrag, Y. Li, S. Wu, M. Cygler, *Nature* **351**, 761 (1991).
53. S. M. Franken, H. J. Rozeboom, K. H. Kalk, B. W. Dijkstra, *EMBO J.* **10**, 1297 (1991).
54. D. L. Ollis *et al.*, unpublished results.
55. B. P. Doctor *et al.*, in *Computer-Assisted Modeling of Receptor-Ligand Interactions. Theoretical Aspects and Applications to Drug Design*, R. Rein and A. Golombek, Eds. (Liss, New York, 1989), vol. 289, pp. 305–316; M. K. Gentry and B. P. Doctor, in *Cholinesterases: Structure, Function, Mechanism, Genetics and Cell Biology*, J. Massoulie *et al.*, Eds. (American Chemical Society, Washington, DC, 1991), pp. 394–398.
56. G. Gibney, S. Camp, M. Dionne, K. MacPhee-Quigley, P. Taylor, *Proc. Natl. Acad. Sci. U.S.A.* **87**, 7546 (1990).
57. T. A. Steitz and R. G. Shulman, *Annu. Rev. Biophys. Bioeng.* **11**, 419 (1982).
58. J. S. Richardson, *Adv. Protein Chem.* **34**, 167 (1981).
59. Y. Maulet *et al.*, *Neuron* **4**, 289 (1990).
60. C. Weise *et al.*, *EMBO J.* **9**, 3885 (1990).
61. B. Kieffer, M. Goeldner, C. Hirth, R. Aebersold, J. Y. Chang, *FEBS Lett.* **202**, 91 (1986).

62. C. Chothia and J. P. Pauling, *Nature* **219**, 1156 (1968).
63. We also fitted the organophosphoryl moiety of monoisopropylphosphoryl-chymotrypsin in a way analogous to that observed in the crystal structure of this conjugate of Cht (M. Harel *et al.*, *J. Mol. Biol.*, in press) with an organophosphate that is also a powerful AChE inhibitor. Determining the structure of similar organophosphate conjugates of AChE itself would help improve our current model of ACh binding and help us map the topography of the active site.
64. J. E. Purdie and R. A. McIvor, *Biochim. Biophys. Acta* **128**, 590 (1966); R. D. O'Brien, *Biochem. J.* **113**, 713 (1969); J. C. Meunier and J. P. Changeux, *FEBS Lett.* **2**, 224 (1969).
65. M. I. Kabachnick *et al.*, *Pharmacol. Rev.* **22**, 355 (1970).
66. G. M. Steinberg, M. L. Mednick, J. Maddox, R. Rice, J. Cramer, *J. Med. Chem.* **18**, 1056 (1975).
67. H. A. Berman and M. M. Decker, *J. Biol. Chem.* **264**, 3951 (1989); H. A. Berman and K. Leonard, *ibid.*, p. 3942.
68. G. Amitai and P. Taylor, in *Cholinesterases: Structure, Function, Mechanism, Genetics and Cell Biology*, J. Massoulie *et al.*, Eds. (American Chemical Society, Washington, DC, 1991), p. 285.
69. H.-J. Nolte, T. L. Rosenberry, E. Neumann, *Biochemistry* **19**, 3705 (1980).
70. J. A. Tainer, E. D. Getzoff, J. S. Richardson, D. C. Richardson, *Nature* **306**, 284 (1983); E. D. Getzoff *et al.*, *ibid.*, p. 287.
71. D. R. Davies and H. Metzger, *Annu. Rev. Immunol.* **1**, 87 (1983).
72. M. Dennis *et al.*, *Biochemistry* **27**, 2346 (1988); J. L. Galzi *et al.*, *J. Biol. Chem.* **265**, 10430 (1990).
73. G. Adam and M. Delbruck, in *Structural Chemistry and Molecular Biology*, A. Rich and N. Davidson, Eds. (Freeman, San Francisco, 1968), pp. 198–215; M. Eigen, in *Quantum Statistical Mechanics in the Natural Sciences*, S. L. Mintz and S. M. Widmayer, Eds. (Plenum, New York, 1974), pp. 37–61.
74. T. L. Rosenberry and E. Neumann, *Biochemistry* **16**, 3870 (1977).
75. A. J. Howard *et al.*, *J. Appl. Crystallogr.* **20**, 383 (1987).
76. W. Kabsch, *ibid.* **21**, 916 (1988).
77. R. E. Dickerson, J. E. Weinzierl, R. A. Palmer, *Acta Crystallogr.* **B24**, 997 (1968).
78. Abbreviations for the amino acid residues are: A, Ala; C, Cys; D, Asp; E, Glu; F, Phe; G, Gly; H, His; I, Ile; K, Lys; L, Leu; M, Met; N, Asn; P, Pro; Q, Gln; R, Arg; S, Ser; T, Thr; V, Val; W, Trp; and Y, Tyr.
79. J. P. Priestle, *J. Appl. Crystallogr.* **21**, 572 (1988).
80. M. Harel, C. T. Su, F. Frolow, I. Silman, J. L. Sussman, *Biochemistry* **30**, 5217 (1991).
81. We thank M. Lachever for help in various stages of this research, O. Herzberg, A. Wlodawer, J. Remington, J. Massoulié, W. Peticolas, B. P. Doctor, D. Ollis, and F. Winkler for valuable discussions, and M. Levitt for his stimulating comments and help in preparing Fig. 7B using the MacIMDAD program. We are also grateful to S. Nidam for his expert photography, O. Bahar for her skilled graphics work, and C. Palustran for help in preparing the manuscript. Supported by U.S. Army Medical Research and Development Command contract no. DAMD17-89-C-9063, the Minerva Foundation, the Revson Foundation, Association Franco-Israélienne pour la Recherche Scientifique et Technologique, the United States–Israel Binational Science Foundation (BSF), Jerusalem, and the Kimmelman Center for Biomolecular Structure and Assembly, Rehovot. I.S. is Bernstein-Mason Professor of Neurochemistry. A.G. is a Markey fellow, and his work on this project was supported by the Lucille P. Markey Charitable Trust. This paper is dedicated to Irwin B. Wilson.

18 April 1991; accepted 12 July 1991

Impact-Induced Cleaving and Melting of Alkali-Halide Nanocrystals

RAINER D. BECK, PAMELA ST. JOHN, MARGIE L. HOMER, ROBERT L. WHETTEN

Impact of nanocrystalline alkali-halide clusters against solid surfaces causes them to fission exclusively into low surface-energy fragments. In time-of-flight scattering experiments, this process appears at an impact energy so low that it must result from a single-step cleavage of the nanocrystal along low surface-energy cleavage planes. At higher energies (more than 1 electron volt per atom), a crossover occurs to an entirely different behavior—evaporative cascades that proceed irrespective of the structure-energetic properties of the fragments. These cascades, and the approximately linear scaling of the crossover energy with cluster size, are characteristic of impact-induced transformation of the cluster to a molten state. Collision with the high-rigidity surface of silicon gives a substantially greater cleavage probability than the soft basal-plane surface of graphite.

IMPACT OF SOLID PROJECTILES AGAINST SOLID SURFACES IS associated with a range of important phenomena (*1*). Sticking or adhesion leads to aggregation and growth of overlayers or the condensed phase. At higher energies, implantation of material into the solid becomes feasible. Ricochet processes include shattering or melting of the scattered projectile. The relative significance of these processes depends upon the effectiveness of the interactions, within and between the projectile and target materials, in accommodating the impact momentum. Investigation of the impact phenomenon of the smallest solids, namely atomic or compound clusters, could allow one to obtain a microscopic understanding of empirical laws governing these phenomena.

Despite a number of reports on scattering of uncharged molecular clusters at hyperthermal energy (*2*) and of mass-selected clusters at much higher energies, (*3*) there has been no well-defined collision experiment, in which the mass and structure of an incident solid cluster are known along with the collision energy and nature of the surface. Of particular interest is the range bounded below by hyperthermal speeds and above by the strongest chemical interactions (approximately 0.05 to 5 eV per atom), where short-range repulsive interactions are dominant (*4*) and implantation or sputtering are unfeasible. Advances in cluster-beam methods (*5*) make it possible to use internally cold, mass-selected cluster beams injected into a scattering chamber under well-defined angular, velocity, and surface conditions. We report studies of collisions of the smallest crystalline objects, specifically the alkali-halide clusters (AHCs), with soft and hard surfaces—highly oriented graphite (0001) and silicon (100)—under conditions fulfilling these criteria.

Cluster formation and acceleration. Ionic compound clusters, including the alkali-halide clusters (AHCs), have the rock-salt ionic bonding of the bulk crystal (*6–12*), that is, they are nanocrystals. Structures of the most stable clusters have cuboid morphology, as shown in Fig. 1, that can be derived from the bulk crystal by cleaving it along mutually perpendicular planes so that only (100) faces are exposed. Less stable clusters are obtained by forming terraces on a

The authors are in the Department of Chemistry, University of California, Los Angeles, CA 90024.